

Magnetic-Field Induced Semimetal in Topological Crystalline Insulator Thin Films

Motohiko Ezawa

We investigate electromagnetic properties of a topological crystalline insulator (TCI) thin film under external electromagnetic fields. The TCI thin film is a topological insulator indexed by the mirror-Chern number. It is demonstrated that the gap closes together with the emergence of a pair of gapless cones carrying opposite chiralities by applying in-plane magnetic field. A pair of gapless points have opposite vortex numbers. This is a reminiscence of a pair of Weyl cones in 3D Weyl semimetal. We thus present an a magnetic-field induced semimetal-semiconductor transition in 2D material. This is a giant-magnetoresistance, where resistivity is controlled by magnetic field. Perpendicular electric field is found to shift the gapless points and also renormalize the Fermi velocity in the direction of the in-plane magnetic field.

Introduction: Topologically stable states such as topological insulator are among the most exciting topics in modern condensed matter physics. Topological crystalline insulator (TCI) is a topological insulator protected by the crystal symmetry¹⁻⁷. Its experimental realizations in $\text{Pb}_x\text{Sn}_{1-x}\text{Te}$ excite studies of TCI⁸⁻¹⁰. A thin film made of TCI provides us with a new platform of 2D electron system^{3,11,12}. When the film is thin enough, the gap opens due to hybridization between the front and back surfaces, and it turns the system into a topological insulator. The TCI thin film is a topological insulator indexed by the mirror-Chern number^{13,14}. Very recently, a TCI thin film made of SnTe was experimentally manufactured¹⁵.

Weyl semimetal¹⁶⁻²⁵ has recently been found to be topologically robust in three dimensions (3D). The emergence of a Weyl semimetal is always accompanied by a pair of Weyl cones with opposite chiralities subject to the fermion doubling theorem²⁶. Each Weyl cone has a gapless point in momentum space, carrying the opposite monopole number. A pair of monopoles cannot annihilate each other dynamically, since they are parts of the ground-state texture of the Berry curvature. The semimetal is topologically stable provided two Weyl cones are separated. Indeed, when two Weyl cones meet head-on by controlling system parameters, they disappear and the gap opens in the system. These are the basic features of the 3D Weyl semimetal.

We investigate the band structure and the topological property of TCI thin film by applying the in-plane magnetic field and the perpendicular electric field. As these external fields are increased, the gap reduces and closes, forming a gapless Dirac cone at certain critical fields. Then the gapless Dirac cone splits into a pair of gapless cones with opposite chiralities. They are akin to a pair of Weyl cones in 3D. Indeed, they carry the opposite vortex numbers. We may call the gapless cone (point) "Weyl" cone (point) in 2D based on the similarity. We find a flat band emerges to connect them in a nanoribbon, as is a reminiscence of the Fermi arc²³ connecting the two Weyl points in the surface of a Weyl semimetal. It is to be emphasized that the emergence of the Weyl points is solely due to the in-plane magnetic field, while the electric field only shifts the position of the Weyl points and renormalizes the Fermi velocity. When we change the direction of in-plane magnetic field, the gap remains open and the positions of the Weyl points rotate in parallel to the magnetic field direction. The pair of Weyl points never annihilate each other provided they

are separated by the in-plane magnetic field. Thus we have presented a magnetic-field induced semimetal-semiconductor transition in 2D material.

Topological Crystalline Insulator Thin Film: Gapless Dirac cones emerge on the surface of a topological insulator. We consider the $[0,0,1]$ TCI surface, where there are gapless Dirac cones at the X and Y points. When the thickness is very thin, the gap opens due to hybridization between the front and back surfaces. We explicitly investigate the low-energy physics near the Fermi energy around the X point, but the same analysis can be carried out also around the Y point. It is well known that the low-energy physics in the vicinity of the Dirac point is described precisely by the Dirac theory. Hence we are able to present analytic formulas. Nevertheless, we also carry out numerical studies based on the tight-binding model to confirm analytical results.

The effective low-energy Hamiltonian of the TCI thin film has been derived in the vicinity of the X point³. It is expressed in terms of 4×4 matrices,

$$H_0 = [v_x k_x \sigma_x - v_y k_y \sigma_y] \tau_y + m \tau_x, \quad (1)$$

where $\sigma = (\sigma_x, \sigma_y, \sigma_z)$ and $\tau = (\tau_x, \tau_y, \tau_z)$ represent the spin and surface degrees of freedom; v_i and k_i are the Fermi velocity and the momentum into the i -direction; $m \tau_x$ represents the tunnelling term between the two surfaces. We have set $\hbar = 1$ for simplicity. The Hamiltonian H_0 has the mirror symmetry, $M H_0(\mathbf{k}) M^{-1} = H_0(\mathbf{k})$, with the generator $M = -\frac{i}{2} \sigma_z \tau_x$.

Without the external fields, the Hilbert space is divided by the eigenvalues ($M = \pm i$) of the mirror operator^{13,14}. The mirror-Chern number C_M is defined by the difference of the Chern numbers in these two sectors. The total Chern number is zero ($C = 0$) and the mirror-Chern number is given by $C_M = \frac{1}{2} \text{sign}(m)$ for each cone. It is a mirror-Chern insulator. When we analyze a nanoribbon based on the tight-binding model¹¹, gapless edge modes appear, as signals the topological nature of the bulk [Fig.1(a)].

We introduce the external field terms

$$H_{\text{ext}} = E_z \tau_z + B_x \sigma_x + B_y \sigma_y. \quad (2)$$

The first term is induced by applying electric field perpendicular to the TCI thin film. The in-plane Zeeman terms are induced by applying in-plane magnetic field.

We explore the system with $H = H_0 + H_{\text{ext}}$. The band structure changes as a function of the external fields. The band

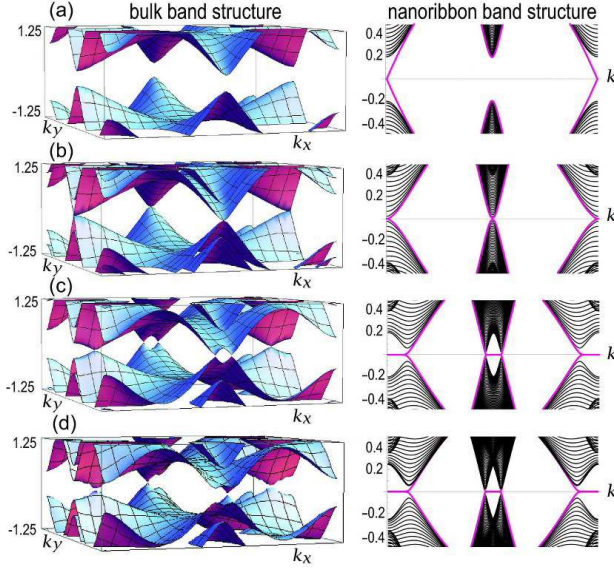


FIG. 1: Band structure of bulk and nanoribbon of the TCI thin film based on the tight-binding model. (a) Without external field ($B_x = 0, B_y = 0$). (b) At the phase transition point ($B_x = m, B_y = 0$), where the band gap closes. (c) In the semimetallic phase ($B_x = 2m, B_y = 0$). (d) In the semimetallic phase ($B_x = 2m, B_y = m$). We have set $m = 0.2$.

gap is located at $k_x = k_y = 0$, where the energy spectrum reads

$$E = \pm \left| \sqrt{B_x^2 + B_y^2} \pm \sqrt{m^2 + E_z^2} \right|. \quad (3)$$

The gap closes when $B_x^2 + B_y^2 = m^2 + E_z^2$, where a topological phase transition occurs [Fig.1(b)].

Before the gap closes the system is an insulator. However, it is no longer a mirror-Chern insulator since the mirror symmetry is broken. When we examine a nanoribbon based on the tight-binding model¹¹, edge modes are gapped. The mirror-Chern number C_M becomes a continuous function of E_z, B_x and B_y and is no longer quantized. For instance, we find²⁷

$$C_M = \frac{m}{2\sqrt{m^2 + E_z^2}}, \quad (4)$$

when we apply only E_z . It is reduced to the quantized value, $C_M = \frac{1}{2}\text{sign}(m)$, in the limit $E_z = 0$.

Magnetic field induced Semimetal: We investigate the TCI thin film after the phase transition point, where the gap closes [Fig.1(c)]. We may choose the direction of the in-plane magnetic field as the x -axis without loss of generality. To study the phenomenon analytically we examine the energy spectrum of the Dirac theory,

$$E = \pm \sqrt{v_y^2 k_y^2 + \left(\sqrt{v_x^2 k_x^2 + m^2 + E_z^2} \pm B_x \right)^2}. \quad (5)$$

We show the band structure in Fig.2. The phase transition point is $B_x^2 = m^2 + E_z^2$. Beyond the point, a gapless Dirac cone is decomposed into two Weyl cones located at $(k_x, k_y) =$

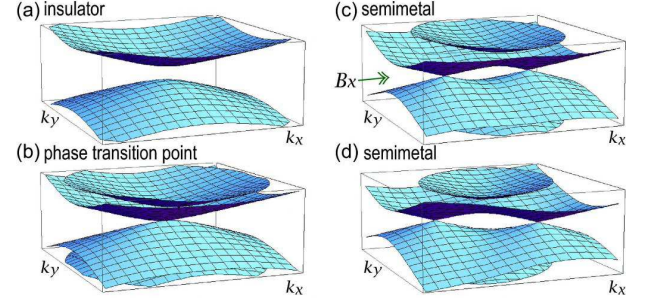


FIG. 2: Band structure near the X point based on the 4-band theory. (a) Without external field ($B_x = 0, B_y = 0$). (b) At the phase transition point ($B_x = m, B_y = 0$), where the band gap closes. (c) In the semimetallic phase ($B_x = 2m, B_y = 0$). (d) In the semimetallic phase ($B_x = 2m, B_y = m$). We have set $m = 0.2$.

$(\pm k_x^X, 0)$ as in Fig.2(c) with $k_x^X = v_x^{-1} \sqrt{B_x^2 - m^2 - E_z^2}$. We also refer to these Weyl points as the X_{\pm} points. It is to be emphasized that the decomposition is made possible by the in-plane magnetic field. We also find that flat edge modes appear connecting the two Weyl points in a nanoribbon [Fig.1(c)], which would correspond to the Fermi arc²³ connecting the two Weyl points in the surface of a 3D Weyl semimetal.

We employ the effective 2×2 Hamiltonian by taking only two bands nearest to the Fermi energy. We may derive it in the second order perturbation theory around the X_{\pm} point as follows. Since the quantization axis is σ_x and τ_x at the Γ point, it is convenient to make the cyclic rotation of the Pauli matrices and diagonalize them. In the new basis the Hamiltonian reads

$$H_0 = [v_x k_x \sigma_z - v_y k_y \sigma_x] \tau_x + m \tau_z + E_z \tau_x + B_x \sigma_z, \quad (6)$$

which is explicitly written as

$$H = \begin{pmatrix} H_1 & T \\ T^\dagger & H_2 \end{pmatrix}, \quad (7)$$

with

$$H_1 = (m - B_x) \sigma_z - v_y k_y \sigma_x, \quad (8)$$

$$H_2 = (-m - B_x) \sigma_z - v_y k_y \sigma_x, \quad (9)$$

$$T = -v_x k_y \sigma_z - i E_z \sigma_y. \quad (10)$$

The dominant term is H_1 . In the second-order perturbation theory, we obtain the effective Hamiltonian

$$\begin{aligned} H_{\text{eff}} &= H_1 - T^\dagger H_2^{-1} T \\ &= (B_x - m - \frac{(m + B_x)(v_x^2 k_x^2 + E_z^2)}{(m + B_x)^2 + v_y k_y^2}) \sigma_z \\ &\quad - v_y k_y (1 + \frac{v_x^2 k_x^2 + E_z^2}{(m + B_x)^2 + v_y k_y^2}) \sigma_x. \end{aligned} \quad (11)$$

By neglecting higher order terms in k_y and changing the Pauli matrices inversely, we obtain the effective Hamiltonian

$$H_{\text{eff}} = \left(B_x - m - \frac{v_x^2 k_x^2 + E_z^2}{m + B_x} \right) \sigma_x - v_y k_y \sigma_y, \quad (12)$$

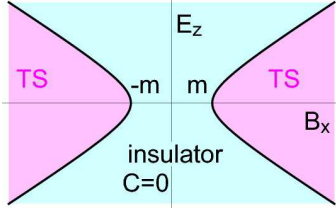


FIG. 3: Topological phase diagram. In the B_x - E_z plane, with the topological semimetal (TS) and the insulator ($C = 0$).

with the energy spectrum being

$$E = \pm \sqrt{\left(\frac{v_x^2 k_x^2 + m^2 + E_z^2 - B_x^2}{m + B_x} \right)^2 + v_y^2 k_y^2}. \quad (13)$$

It agrees with (5) up to the order of k_x^4 .

At the transition point $B_x^2 = m^2 + E_z^2$ [Fig.2(b)], the energy spectrum is highly anisotropic. The dispersion is Schrödinger-like in the k_x direction, and Dirac-like in the k_y direction.

Beyond the transition point $B_x^2 > m^2 + E_z^2$ [Fig.2(c)], we rewrite the Hamiltonian (12) as

$$H_{\text{eff}} = -\frac{v_x^2 (k_x - k_x^X) (k_x + k_x^X)}{m + B_x} \sigma_x - v_y k_y \sigma_y. \quad (14)$$

We may approximate $k_x \pm k_x^X = \pm 2k_x^X$ around the X_{\pm} point,

$$H_{\text{eff}}^{X_{\pm}} = \mp \tilde{v}_x (k_x \mp k_x^X) \sigma_x - v_y k_y \sigma_y, \quad (15)$$

with the renormalized velocity $\tilde{v}_x = 2v_x^2 k_x^X / (m + B_x)$. The energy spectrum in the vicinity of the X_{\pm} points is

$$E_{\pm} = \pm \sqrt{\tilde{v}_x^2 k_x^2 + v_y^2 k_y^2}. \quad (16)$$

The role of E_z is to shift the position of the Weyl points and renormalize the Fermi velocity.

It is easy to consider the general in-plane field $B_x \neq 0$ and $B_y \neq 0$ when $E_z = 0$. We find that the gap closes at (k_x^X, k_y^X) and $(-k_x^X, -k_y^X)$, where

$$(k_x^X, k_y^X) = (v_x^{-1} |B_x|, v_y^{-1} |B_y|) / \sqrt{1 - m^2/B_{\parallel}^2}, \quad (17)$$

with $B_{\parallel}^2 = B_x^2 + B_y^2$. The positions of Weyl cones are parallel to the direction of the magnetic field. We have also confirmed the results by calculating the band structure of the bulk and a nanoribbon based on the tight-binding model. Namely the gap remains closed for an arbitral direction of the in-plane field, as we show an example in Fig.1(e).

We discuss the topological stability of the X_{\pm} points. The Hamiltonian is of the form

$$H_{\text{eff}} = R(n_x \sigma_x + n_y \sigma_y), \quad (18)$$

where n_x and n_y are normalized fields subject to $n_x^2 + n_y^2 = 1$. It has two eigen-spinors with the eigen-energy $E_{\pm} = \pm |R|$.

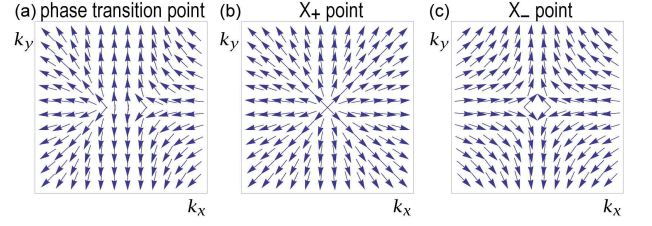


FIG. 4: Spin direction based on the 2-band theory. (a) In the topological insulator ($M_x = 0$). (b) At the transition point ($M_x = m$). (c) In the topological semimetal ($M_x = 2m$), where a hedgehog structure is found at the X_+ point, and an anti-hedgehog structure at the X_- point. The vortex number is nontrivial at these points.

The state corresponding to the filled band is given by the spinor

$$|S\rangle = \frac{1}{\sqrt{2}} \begin{pmatrix} e^{-i\phi/2} \\ -e^{+i\phi/2} \end{pmatrix}, \quad (19)$$

when we parametrize $(n_x, n_y) = (\cos \phi, \sin \phi)$. The spin of the state is given by $s_i = \langle S | \sigma_i | S \rangle$, which we show in Fig.4. We note that $s_i = -n_i$. The spin direction forms a hedgehog structure in the vicinity of the X_+ point, while it forms an anti-hedgehog structure in the vicinity of the X_- point. There are a source and a sink of the spin flow at these points. They are described by a topological charge.

We may define the vortex number for the spin texture by²⁸

$$Q = \frac{1}{2\pi} \oint dk_{\alpha} [s_x(\mathbf{k}) \partial_{k_{\alpha}} s_y(\mathbf{k}) - s_y(\mathbf{k}) \partial_{k_{\alpha}} s_x(\mathbf{k})], \quad (20)$$

where the integration is carried out along the boundary of the Brillouin zone. It is trivial to see

$$Q = \frac{1}{2\pi} \oint dk_{\mu} \partial_{k_{\mu}} \phi. \quad (21)$$

In general, it yields $Q = 0, \pm 1, \pm 2, \dots$, because ϕ is defined only modulo 2π . For the specific field configuration given in (15), we find $Q = \pm 1$ for the Weyl cones at X_{\pm} . These values are topologically stable because any perturbation cannot change the quantized value of the topological charge Q . We may also evaluate the topological number for the spin configuration at the phase transition point [Fig.4(a)] and also before the phase transition point (i.e. in the insulator phase) to find that $Q = 0$. We may interpret that a pair creation of Weyl cones with $Q = \pm 1$ occurs from the topological trivial Dirac cone with $Q = 0$ at the phase transition point. It is interesting to note that a flat edge mode appear to connect the two X_{\pm} points in a nanoribbon [Fig.1(c)]. Note that the total topological charge (20) is zero ($Q = 0$) both before and after the phase transition. Nevertheless, the semimetallic phase is stable topologically due to the presence of a pair of two Weyl cones with $Q = \pm 1$ generated by the in-plane field, precisely as in the 3D Weyl semimetal.

The same analysis is carried out for the Dirac cone at the Y point, from which a pair of Weyl cones emerge located at the Y_{\pm} point under in-plane magnetic field.

Discussions: We have demonstrated that a semimetallic phase emerges in a TCI thin film by applying in-plane magnetic field. The semimetallic phase is characterized by the existence of a pair of gapless Weyl cones as in the case of the 3D Weyl semimetal. In conclusion, we have proposed a magnetic-field induced semimetal-semiconductor transition in 2D material. This is a giant-magnetoresistance, where resistivity is controlled by magnetic field. The transition between the insulator phase and the semimetallic phase will be exper-

imentally detectable by electric transport measurement. The TCI thin film has already been manufactured¹⁵. Our finding will open a way to magneto-nanoelectronics based on the TCI thin film.

I am very much grateful to N. Nagaosa, Y. Ando and Y. Tanaka for helpful discussions on the subject. This work was supported in part by Grants-in-Aid for Scientific Research from the Ministry of Education, Science, Sports and Culture No. 25400317.

-
- ¹ L. Fu, Phys. Rev. Lett. 106, 106802 (2011).
 - ² T. H. Hsieh, H. Lin, J. Liu, W. Duan, A. Bansil and L. Fu, Nat. Comm. 3, 982 (2012).
 - ³ J. Liu, et.al. Nat. Mat. 13 178 (2014).
 - ⁴ C. Fang, M. J. Gilbert, B. A. Bernevig, Phys. Rev. Lett. 112, 046801 (2014).
 - ⁵ J. Liu, W. Duan and L. Fu, Phys. Rev. B 88 241303(R) (2013).
 - ⁶ Y. Okada, M. Serbyn, H. Lin, D. Walkup, W. Zhou, C. Dhital, M. Neupane, S. Xu, Y. J. Wang, R. Sankar, F. Chou, A. Bansil, M. Z. Hasan, S. D. Wilson, L. Fu, V. Madhavan, Science 341 1496 (2013).
 - ⁷ M. Ezawa, Phys. Rev. B 89, 195413 (2014).
 - ⁸ Y. Tanaka, Z. Ren, T. Sato, K. Nakayama, S. Souma, T. Takahashi, K. Segawa and Y. Ando, Nat. Phys. 8, 800 (2012).
 - ⁹ Su-Yang Xu, Chang Li, N. Alidoust, M. Neupane, D. Qian, I. Belopolski, J.D. Denlinger, Y.J. Wang, H. Lin, L.A. Wray, G. Landolt, B. Slomski, J.H. Dil, A. Marcinkova, E. Morosan, Q. Gibson, R. Sankar, F.C. Chou, R. J. Cava, A. Bansil and M.Z. Hasan, Nat. Com. 3, 1192 (2012).
 - ¹⁰ P. Dziawa, B. J. Kowalski, K. Dybko, R. Buczko, A. Szczerbakow, M. Szot, E. Lusakowska, T. Balasubramanian, B. M. Wojek, M. H. Berntsen, O. Tjernberg and T. Story, Nat. Mat. 11, 1023 (2012).
 - ¹¹ M. Ezawa, New J. Phys. 16, 065015 (2014).
 - ¹² H. Ozawa, A. Yamakage, M. Sato, Y. Tanaka, Phys. Rev. B 90, 045309 (2014).
 - ¹³ Jeffrey C.Y. Teo, Liang Fu, C.L. Kane, Phys. Rev. B 78, 045426 (2008).
 - ¹⁴ R. Takahashi and S. Murakami, Phys. Rev. Lett. 107, 166805 (2011).
 - ¹⁵ A. A. Taskin, F. Yang, S. Sasaki, K. Segawa, and Y. Ando, Phys. Rev. B 89, 121302(R) (2014).
 - ¹⁶ S. Murakami, New J. Phys. 9, 356 (2007).
 - ¹⁷ P. Hosur, X. L. Qi, Comptes Rendus Physique 14, 857 (2013).
 - ¹⁸ T. O. Wehling, A. M. Black-Schaffer, and A. V. Balatsky, Adv. Phys. 76, 1 (2014).
 - ¹⁹ O. Vafek, A. Vishwanath, Ann. Rev. Cond. Mat. Phys. 5, 83 (2014).
 - ²⁰ A.A. Burkov and L. Balents, Phys. Rev. Lett. 107, 127205 (2011).
 - ²¹ P. Hosur, S. A. Parameswaran, and A. Vishwanath, Phys. Rev. Lett. 108, 046602 (2012).
 - ²² Gabor B. Halasz and L. Balents, Phys. Rev. B 85, 035103 (2012).
 - ²³ X. Wan, A. M. Turner, A. Vishwanath, and S. Y. Savrasov, Phys. Rev. B 83, 205101 (2011).
 - ²⁴ A. A. Zyuzin and A. A. Burkov, Phys. Rev. B 86, 115133 (2012).
 - ²⁵ A. Sekine, K. Nomura, J. Phys. Soc. Jpn. 82, 033702 (2013).
 - ²⁶ H. B. Nielsen and M. Ninomiya (1981) Phys. Lett. B 105, 219.
 - ²⁷ M. Ezawa, Phys. Lett. A 378, 1180 (2014).
 - ²⁸ M. Ezawa, Phys. Rev. B 83, 100408(R) (2011).